DOI: 10.1021/cg900943x

CRYSTAL GROWTH & DESIGN Article

2010, Vol. 10 357–364

Stepwise Topotactic Transformations (1D to 3D) in Copper Carboxyphosphonate Materials: Structural Correlations

Konstantinos D. Demadis,*[,#] Maria Papadaki,[#] Miguel A. G. Aranda,*[,‡] Aurelio Cabeza,[‡] Pascual Olivera-Pastor,[‡] and Yiannis Sanakis[§]

[#]*Crystal Engineering, Growth and Design Laboratory, Department of Chemistry, University of Crete, Voutes Campus, Crete, GR-71003, Greece,* [‡]*Departamento de Química Inorgánica, Universidad de Málaga, Campus Teatinos S/N 29071-Málaga, Spain, and* [§]*Institute of Materials Science, NCSR "Demokritos", 15310 Ag. Paraskevi Attikis, Greece*

Received August 10, 2009; Revised Manuscript Received October 20, 2009

ABSTRACT: In this report, we demonstrate a topotactic transformation of a $[Cu(HPAA)(H_2O)_2]\cdot H_2O$ one-dimensional (1D) hybrid (HPAA = $HO_3PCH(OH)CO_2$, hydroxyphosphonoacetate dianion) to an anhydrous Cu(HPAA) three-dimensional (3D) framework, via the 1D intermediate $Cu(HPAA)(H_2O)_2$. Removal of lattice water from 1D $[Cu(HPAA)(H_2O)_2]\cdot H_2O$ yields 1D $Cu(HPAA)(H_2O)_2$ and results in alterations in hydrogen bonding interactions (chain$\cdots H_2O\cdots$chain), and, in turn, compaction of the chains as well as "slipping". These changes are accompanied by creation of a new hydrogen bonding scheme (chain$\cdots$chain) involving the phosphonate groups and the hydroxyl/carboxy moieties. The initial zigzag 1D chain is retained throughout the dehydration process. In 3D Cu(HPAA) the resulting vacant sites on Cu (generated by removal of both Cu-bound waters) are occupied by phosphonate oxygens from neighboring chains. All three materials have been characterized by X-ray diffraction and a variety of other techniques and their structures have been determined.

Introduction

Research in supramolecular chemistry and crystal engineering has been advanced thanks to the availability of a plethora of suitable multifunctional ligands.[1] Predominant among these are carboxylate-,[2] (imid- or pyr-)azole-,[3] polypyridyl-,[4] and organoborate[5] based ligands. In particular, materials that contain polyphosphonate building blocks have been investigated intensely for some time now.[6] Part of these investigations concern bifunctional carboxyphosphonate ligands, in which phosphonate and carboxylate moieties are present in the same ligand backbone.[7] Examples of such "mixed" phosphonate/carboxylate ligands are shown schematically in Scheme 1.

Topotactic transformations among crystalline inorganic−organic coordination polymers and other complexes have been demonstrated for a number of systems.[8] For example, two compounds, $CoCl_2$(1,4-dioxane)$(H_2O)_2$ and $CoCl_2$(1,4-dioxane), undergo a crystal-to-crystal transformation from one-dimensional (1D) chains in the former into a three-dimensional (3D) diamondoid network in the latter accompanied by a drastic change in magnetic properties.[8a] Reversible crystal-to-crystal cross-linking of a ribbon of Co-citrate cubanes to form a two-dimensional (2D) net were reported.[8b] Reversible crystal-to-crystal dehydration accompanied by channel formation was reported for calixarene-based architectures.[8c] Another reversible crystal-to-crystal transformation from achiral hexanuclear clusters $[\{Fe^{III}(Tp)(CN)_3\}_4\{Fe^{II}(MeCN)(H_2O)_2\}_2]\cdot 10H_2O\cdot 2MeCN$ (1) (Tp = hydrotris(pyrazoly)borate) to a chiral 1D double zigzag chain via generation/cleavage of coordination bonds was reported and involves the reversible change in magnetization between antiferromagnetic in a zero-dimensional (0D) cluster and ferrimagnetic in a 1D chain.[8d]

Framework interconversions and topotactic transformations are much less known in metal phosphonate chemistry.[9] Some notable examples follow. Depending on the acidity of the reaction medium, $Ba(HOOCC_6H_4PO_3H)_2$ can be converted to $Ba_3(OOCC_6H_4PO_3)_2\cdot 2H_2O$ and vice versa. As an intermediate in these reactions, $BaH(OOCC_6H_4PO_3)$ is formed.[9a] Similar interconversion chemistry was reported for the Sr^{2+} analogue.[9b] Our research groups have recently reported a reversible dehydration/hydration process and ammonia uptake in a calcium tetraphosphonate 2D layered hybrid.[10]

Metal phosphonate materials that contain either metal-bound or interstitial water molecules are ideal candidates for dehydration-induced framework transformations. A prerequisite, however, is that after the dehydration step no framework collapse ensues. Thermogravimetry is a useful technique in assaying the stability of the framework after the loss of volatile molecules. Hence, in this report we demonstrate a dehydration-induced topotactic transformation of a hydrated $[Cu(HPAA)(H_2O)_2]\cdot H_2O$ 1D hybrid (HPAA = $HO_3PCH(OH)CO_2$, hydroxyphosphonoacetate dianion) to an anhydrous Cu(HPAA) 3D framework, via the 1D intermediate $Cu(HPAA)(H_2O)_2$. All these materials have been characterized by X-ray diffraction and a variety of other techniques and their structures have been determined.

Experimental Section

The designation **Cu-L-x-y-nD** is followed throughout the manuscript, where **L** is the ligand dianion $HPAA^{2-}$, **x** is the number of copper-bound water molecules, **y** is the number of lattice water molecules, and **n** is the dimensionality of the framework. Thus, for the three compounds discussed herein, the following designation is used:

$Cu(HPAA)(H_2O)_2]\cdot H_2O$	**Cu-L-2-1-1D**
$[Cu(HPAA)(H_2O)_2]$	**Cu-L-2-0-1D**
$[Cu(HPAA)]$	**Cu-L-0-0-3D**

Synthetic Details. Compound **Cu-L-2-1-1D** was prepared according to a recently published procedure.[11] Compound **Cu-L-2-0-1D**

*Corresponding authors. E-mail: demadis@chemisry.uoc.gr (K.D.D.); g_aranda@uma.es (M.A.G.A.).

Published on Web 12/04/2009

Scheme 1. Some Representative Schematic Structures of Ligands That Possess Both Carboxylic and Phosphonic Acid Moieties in Their Backbone[a]

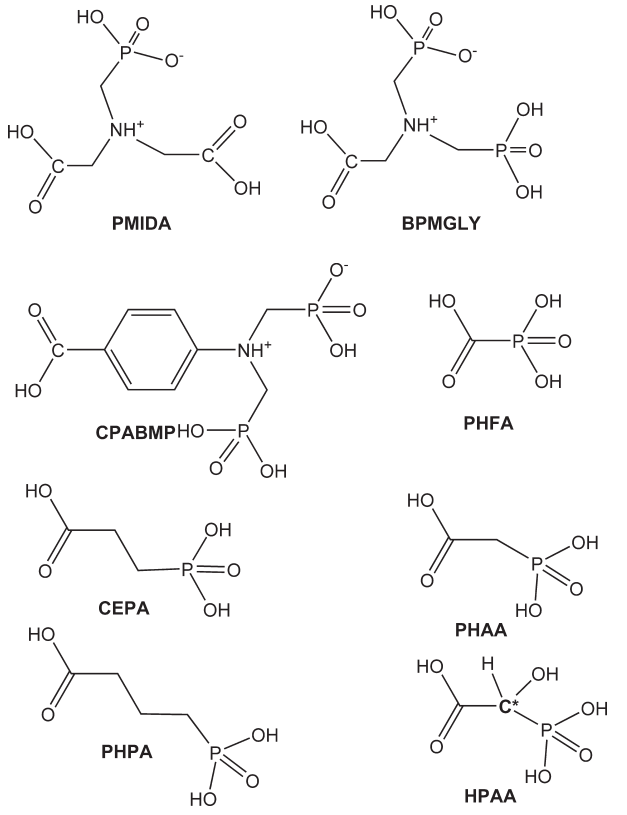

[a] Abbreviations: PMIDA = phosphonomethyliminodiacetic acid, BPMGLY = Bis(phosphonomethyl)glycine, CPABMP = 4-carboxyphenyl-1-amino-bis(methylenephosphonic acid), CEPA = carboxyethylphosphonic acid, PHPA = phosphonopropionic acid, PHFA = phosphonoformic acid, PHAA = phosphonoacetic acid, HPAA = hydroxyphosphonoacetic acid (the * indicates the presence of a chiral carbon).

was prepared by gently heating **Cu-L-2-1-1D** at 55−70 °C for ~2 h. Compound **Cu-L-0-0-3D** was prepared quantitatively by heating a sample of **Cu-L-2-1-1D** under air at 120 °C for 2 h.

Thermodiffractometry and X-ray Powder Diffraction. The thermodiffractometric study for **Cu-L-2-1-1D** was carried out using an Anton Paar TTK1200N camera along a continuous flux (0.02 $L \cdot min^{-1}$) of *dry* He as inert gas. At this point, it is important to note that the humidity in the chamber is only 34.7 deg and it is undersaturated in water vapor. This will be important in the discussion on the behavior of the reported materials, later in the manuscript. The data were collected using a Bragg−Brentano configuration, with a Ge(111) primary monochromator (Cu $K\alpha_1$ radiation) and X'Celerator detector working with maximum active length. The sample, loaded in an alumina sample holder, was heated at small intervals (20 °C) from room temperature to 170 °C with a delay time of 10 min in order to ensure thermal equilibration. The data range was 7−40° (2θ), step size of 0.017°, and an equivalent counting time of 81 s/step. Afterward, the temperature was dropped to 30 °C and a new set of data was collected to carry out the structure determination of dehydrated **Cu-L-0-0-3D** (13−110° (2θ), step size of 0.017°, and an equivalent counting time of 611 s/step).

The X-ray powder diffraction (XRPD) pattern of **Cu-L-0-0-3D** for indexing purposes was collected between 13 and 70° (2θ) (step size of 0.017° and 611 s/step), with the sample loaded in a flat aluminum holder, using a Bragg−Brentano configuration with Ge(111) primary monochromator (Cu $K\alpha_1$ radiation) and X-'Celerator detector. This configuration minimizes the zero-error which is very important for the success in the indexing step. The pattern was autoindexed in an orthorhombic cell using the program DICVOL06.[12] The unit cell obtained was a = 8.613(1) Å, b = 9.894(1) Å, c = 11.733(1) Å, V = 999.9 $Å^3$, $V_{non\text{-}Hatom}$ = 12.5 $Å^3$ $atom^{-1}$, M_{20} = 79 and F_{20} = 136(0.0030, 49).[13,14] The systematic extinctions were consistent with the space group *Pbca*.

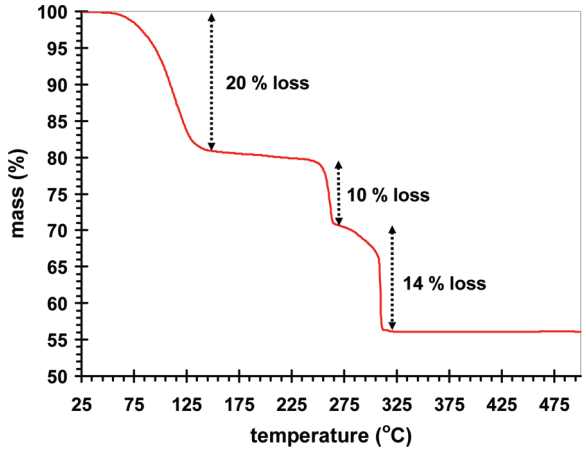

Figure 1. The TGA curve is displayed for the compound **Cu-L-2-0-1D**.

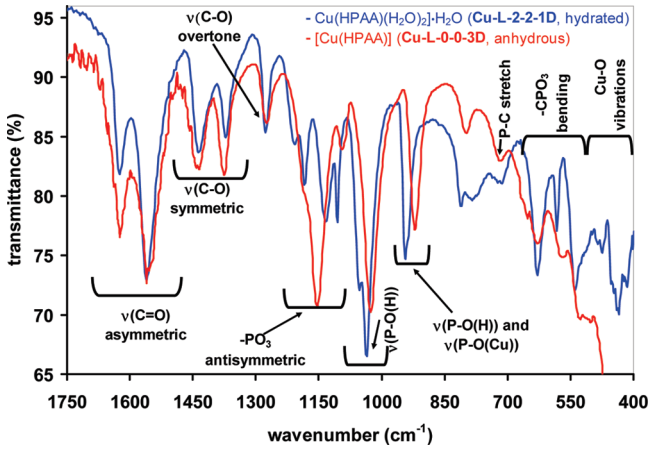

Figure 2. FT-IR spectra of **Cu-L-2-1-1D** (blue) and its anhydrous form **Cu-L-0-0-3D** (red).

The crystal structure of **Cu-L-0-0-3D** was solved using the program EXPO2004[15] by default setting, which gave all atoms present in the asymmetric unit. The structural model obtained was refined by the Rietveld method,[16] with the GSAS package,[17] and using soft constraints to keep a chemically reasonable geometries for the phosphonate and carboxylic groups. The soft constraints were /PO_3C_1 tetrahedron/ P−O [1.53(1) Å], P−C_1 [1.80(1) Å], O···O [2.55(2) Å], O···C_1 [2.73(2) Å], /C_1OH-C_2OO group/ C_1−C_2 [1.50(1) Å], C_2−O_{carb} [1.23(1) Å], C_1−OH [1.40(1) Å], P···OH [2.68(2) Å], C_2−OH [2.40(2) Å], O_{carb}···O_{carb} [2.21(2) Å] and C_1···O_{carb} [2.36(2) Å]. The final weight factor for the soft constraint histogram was 20. Severe preferred orientation effects were not observed, and a small contribution along the [001] direction was modeled using the March-Dollase correction.[18] Finally, only two independent U_{iso} parameters were refined: one for Cu and another for P, C, and O.

The XRPD pattern of **Cu-L-2-0-1D** for the structural characterization was recorded as described above for **Cu-L-0-0-3D**. The pattern was also autoindexed in an orthorhombic cell with systematic extinctions consistent with the space group *Pbca*. The structure of **Cu-L-2-0-1D** has been obtained by Rietveld refinement using as starting model the reported structure of **Cu-L-2-1-1D** from single crystal data[11] and removing the lattice water. The atomic parameters were optimized subjected to the soft-constraints given above for **Cu-L-2-0-1D**.

The crystal structure of **Cu-L-2-0-1D** was deposited at CCDC with the reference code 735500 and that of **Cu-L-0-0-3D** with the reference code 673502.

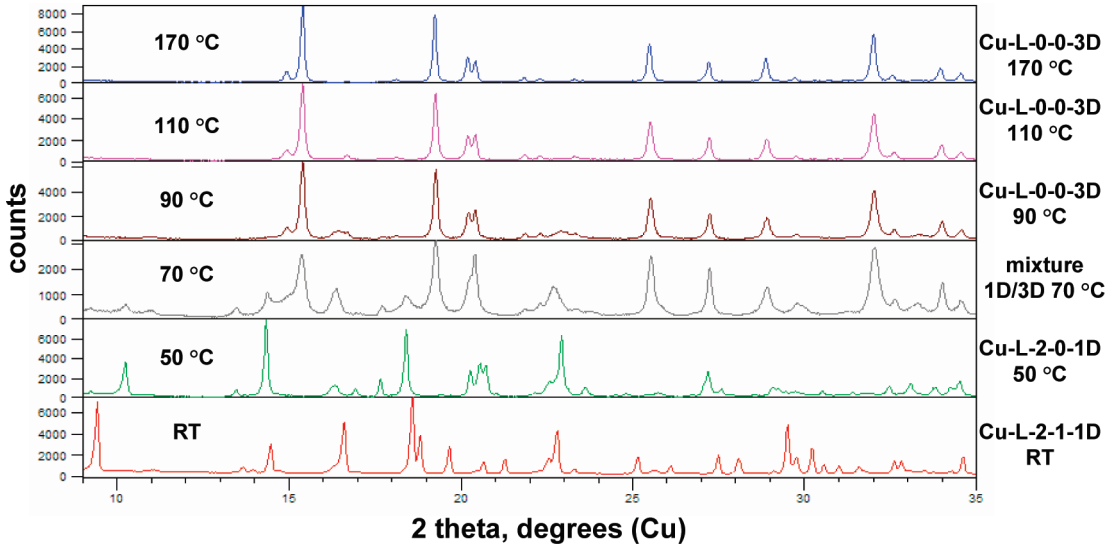

Figure 3. Thermodiffractometric study of the transformation of $[Cu(HPAA)(H_2O)_2]\cdot H_2O$ (**Cu-L-2-1-1D**, RT), to $[Cu(HPAA)(H_2O)_2]$ (**Cu-L-2-0-1D**, 50 °C), to Cu(HPAA) (**Cu-L-0-0-3D**, > 70 °C).

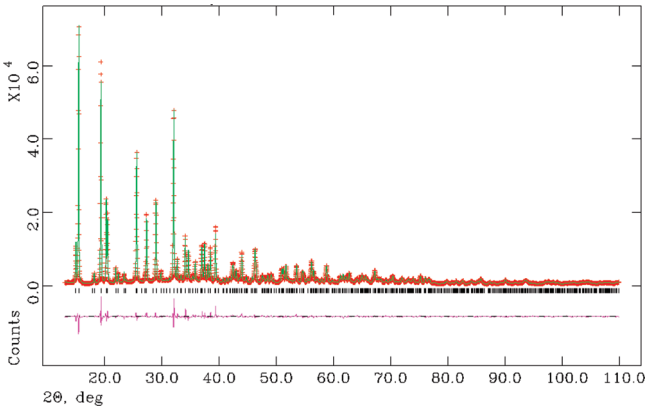

Figure 4. Final observed (crosses), calculated (solid line), and difference plots for the Rietveld refinement of XRPD data for **Cu-L-0-0-3D**. The vertical bars highlight the positions of the diffraction peaks allowed by the *Pbca* space group.

Thermogravimetric and FT-IR Studies. The TGA apparatus was a TGA/SDTA 851-LF 1100-Mettler, with the carrier gas being either air or N_2 at a flow of 100 mL/min. Samples were heated from 25 to 800 °C, at a heating rate of 7 °C/min in an aluminum pot (volume 30 μL). FT-IR spectra were recorded on a FT-IR Perkin−Elmer FT 1760.

Magnetic and EPR Studies. Variable-temperature magnetic susceptibility measurements were carried out on polycrystalline samples of "hydrated" and "anhydrous" complexes in the 5.0−300 K temperature range using a Quantum Design MPMS SQUID magnetometer under a magnetic field of 0.1 T. Diamagnetic corrections for the complexes were estimated from Pascal's constants. X-band EPR measurements were carried out with an upgraded Bruker ER-200D spectrometer equipped with an Anritsu frequency counter, an NMR Gaussmeter and an Oxford ESR-9 cryostat.

Results and Discussion

On the basis of the thermogravimetric study (Figure 1) **Cu-L-2-1-1D** is stable to ~50 °C, after which it quickly loses the water molecules up to 150 °C. The loss of ~20.0% (calculated 19.9%) corresponds well to loss of both Cu-coordinated waters and the water of crystallization, all three in one step under the TGA experimental conditions. Beyond 150 °C the material decomposes in two steps (250−270 °C and 300−315 °C). The total observed mass loss of ~44% corresponds well to the calculated 42% (based on the formation of $Cu_2P_2O_7$ which was identified by its powder diffraction pattern, PDF-79-2075). The TGA was carried out under either air or N_2, without any difference in results.

There is a "dynamic" temperature "window" from ~125 to ~250 °C where no mass loss is observed. This product that has lost all three water molecules was first studied by FT-IR

Table 1. Selected Bond Distances (Å) Cu-L-0-0-3D

Bond Distances (Å)	
Cu−O(1) 1.994(4)	P−O(1) 1.510(4)
Cu−O(3) 1.988(4)	P−O(2) 1.571(4)
Cu−OC(2) 2.036(5)	P−O(3) 1.526(3)
Cu−OC(1) 2.001(5)	P−C(1) 1.842(4)
Cu−O(H) 2.280(5)	C(1)−C(2) 1.526(5)
Cu−O(1) 2.617(5)[a]	C(1)−O(H) 1.404(5)
C(2)−OC(1) 1.263(5)	C(2)−OC(2) 1.232(5)
Angles (in deg)	
O(1)−Cu−O(3)	94.80(18)
O(1)−Cu−OC(2)	89.35(18)
O(1)−Cu−OC(1)	171.66(19)
O(3)−Cu−OC(2)	173.86(19)
O(3)−Cu−OC(1)	88.44(19)
OC(2)−Cu−OC(1)	86.85(19)

[a] O(1) is symmetry related to the previous O(1) by −x − y − z.

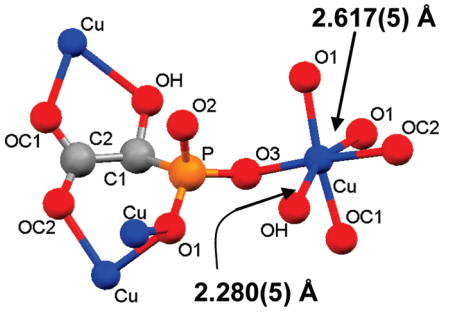

Figure 5. The basic building unit in the framework **Cu-L-0-0-3D**, showing the Jahn−Teller elongation in the Cu−O bond distances. Color codes: Cu blue, P orange, O red, C gray.

spectroscopy in order to establish that it contains Cu-bound HPAA. The FT-IR spectrum is shown in Figure 2, along with the spectrum of the initial, hydrated compound. There are some notable similarities, as well as significant differences in the two spectra. The regions 1470−1690 cm^{-1}, where the $\nu(C{=}O)_{asym}$ stretches appear, and 1300−1470 cm^{-1}, where the $\nu(C{-}O)_{sym}$ appear, are identical for both compounds. This is a strong indication that the carboxylate binding is the same in both compounds. Peak shifts and intensity differences are evident in the spectral region where bands due the phosphonate moiety appear, 880−1250 cm^{-1}.[19] In turn, these observations are an indication that the Cu-phosphonate binding motif in **Cu-L-0-0-1D** is different from that in **Cu-L-0-0-3D**. As will be discussed later, these observations have been verified by structural analysis of **Cu-L-0-0-3D**.

A thermodiffractometric study was also carried out in order to study the transformation of the fully hydrated **Cu-L-2-1-1D** to the anhydrous **Cu-L-0-0-3D** form and its temperature dependence. The results are shown in Figure 3. The room temperature XRPD pattern of compound **Cu-L-2-1-1D** starts to change even at 30 °C, indicating the formation of a new phase. As will be shown later this phase is **Cu-L-2-0-1D** (which have lost only the lattice water). Temperature increase to 70 °C results into the initiation of the final step of the dehydration process and is demonstrated by the appearance of new diffraction peaks. Conversion of **Cu-L-2-1-1D** to the new phase **Cu-L-0-0-3D** is complete at 110 °C. Beyond this temperature and up to 170 °C no further change is observed.

The high crystallinity of **Cu-L-0-0-3D** allowed successful structure solution and Rietveld refinement. The observed and calculated patterns are given in Figure 4. The refinement is satisfactory as evidenced by the low *R*-factors (R_{WP} = 0.067 and R_F = 0.020) and the flatness of the divergence curve; see Figure 4. Selected bond distances and angles for **Cu-L-0-0-3D** are given in Table 1.

The asymmetric unit of **Cu-L-0-0-3D** is shown in Figure 5. The Cu^{2+} center is located in an axially elongated octahedral environment. The "long" bonds are Cu−O(1)(phosphonate) 2.617(5) Å and Cu−OH (hydroxyl) 2.280(5) Å. The $HPAA^{2-}$ ligand coordinates to four Cu^{2+} cations with four different coordination modes: (a) the hydroxyl and carboxyl oxygens generate a five-membered chelate ring; (b) one oxygen from the carboxylate unit and another from the phosphonate group forms a six-membered chelate ring; (c) the O(3) oxygen (from the phosphonate group) coordinates terminally to one Cu^{2+}; and (d) the O(1) oxygen (from the phosphonate group) also acts as a bridge between two Cu^{2+} cations generating infinite Cu−O(1)−Cu chains. The noncoordinated P−O(2) group is the hydrogenphosphonate, P−OH, moiety because the P−O bond length is 1.571(4) Å, longer than the other two P−O bond distances of 1.510(4) and 1.526(3) Å.

Various views of the structure of **Cu-L-0-0-3D** are shown in Figure 6. **Cu-L-0-0-3D** is a 3D coordination polymer with a dense structure.

Intermediates during the Cu-L-2-1-1D → Cu-L-0-0-3D Transformation. There is one lattice water in the structure of **Cu-L-2-1-1D**.[11] Its removal is accompanied by formation of a new crystalline phase, as indicated by the

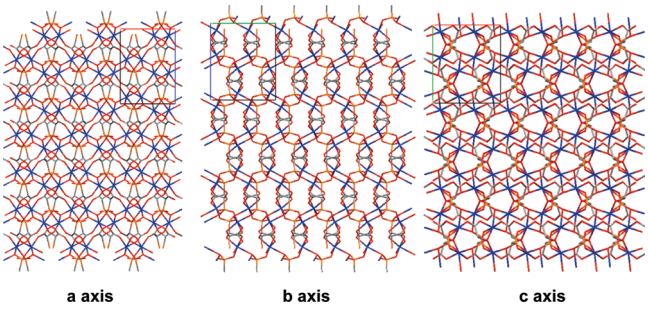

Figure 6. Views of the crystal structure of **Cu-L-0-0-3D** along the *a*, *b*, and *c* axes.

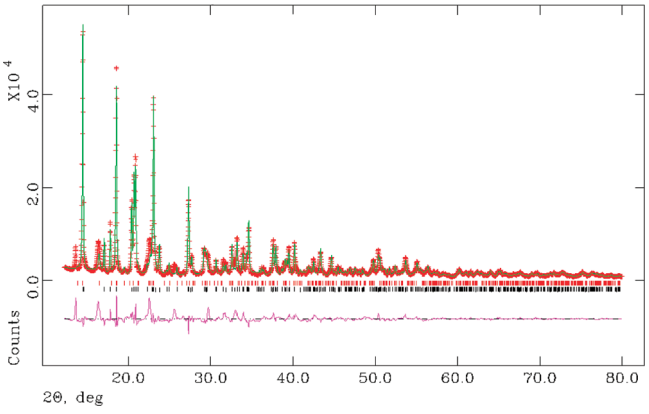

Figure 7. Final observed (crosses), calculated (solid line), and difference plots for the Rietveld refinement of XRPD data for **Cu-L-2-0-1D** sample. The vertical bars highlight the positions of the allowed diffraction peaks including those arising from a small fraction of **Cu-L-2-1-1D**, which has much broader diffraction peaks.

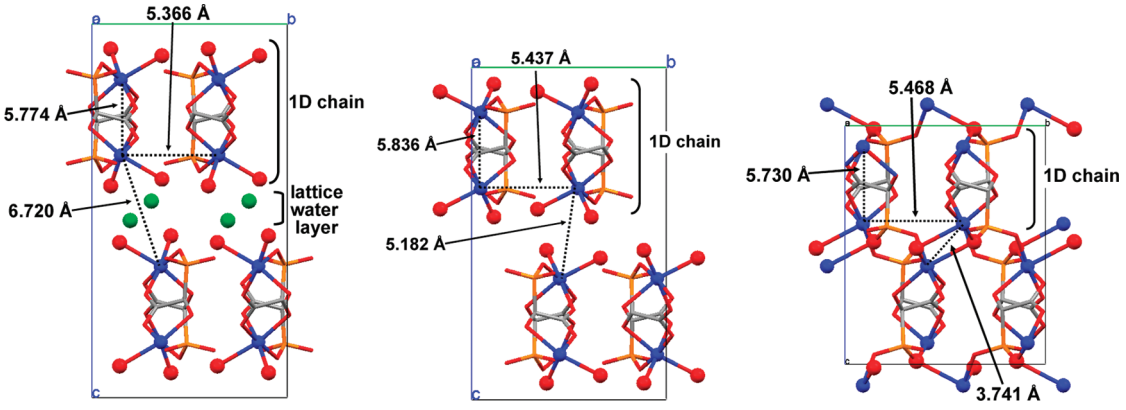

Figure 8. Changes in packing between the 1D zigzag chains upon removal of the lattice water molecule and subsequent removal of Cu-bound waters (**Cu-L-2-1-1D** left, **Cu-L-2-0-1D** middle, **Cu-L-0-0-3D** right). Salient features are shown. The color codes are the same as in Figure 5. Lattice water is colored green. Note the gradual reduction in the *c*-axis length.

thermodiffraction data in Figure 3. It is reasonable to assume that this is the first step in the complete dehydration process to remove all three waters from **Cu-L-2-1-1D** and yield the completely anhydrous phase **Cu-L-0-0-3D**. In an effort to characterize possible intermediates during the removal of all three waters (one lattice, and two Cu-bound) from **Cu-L-2-1-1D**, we attempted to remove exclusively the lattice water by "gently" heating a sample of **Cu-L-2-1-1D**. Indeed, an intermediate phase was identified, which is $[Cu(HPAA)(H_2O)_2]$, **Cu-L-2-0-1D**. Its structure was revealed by Rietveld analysis of powder diffraction data (see Figure 7).

As expected, the 1D zigzag chain in **Cu-L-2-1-1D** has been retained in **Cu-L-2-0-1D**, and only the lattice water has been removed; see Figure 8, left and middle. The lattice water holds the chains together via hydrogen bonding; therefore, its removal is expected to alter the hydrogen bonding scheme, and ultimately cause a partial "collapse" of the structure, bringing the chains closer together. This denser packing of the chains is demonstrated visually in Figure 8 (middle) and also by a notable, nearly 2 Å *c*-axis length reduction from 18.924(5) Å in **Cu-L-2-1-1D**, to 17.011(1) Å in **Cu-L-2-0-1D**. The denser packing in **Cu-L-2-0-1D** (induced by lattice water loss) is also accompanied by further changes. This is due to the dramatic alteration of the hydrogen bonding scheme that positions the chains ~ 6.720 Å apart (Cu···Cu distance, see Figure 8, left). The lattice waters located between the chains in **Cu-L-2-1-1D** each form four hydrogen bonds, two with the Cu-coordinated phosphonate oxygen and two with the Cu-coordinated waters. Upon removal of lattice waters the chains in **Cu-L-2-0-1D** are now held by two hydrogen bonds. One is between one Cu-bound water and a Cu-bound phosphonate oxygen (O···O distance 2.823 Å). The second H-bond is between the other Cu-bound water and a phosphonate oxygen that is not coordinated to Cu (O···O distance 2.817 Å).

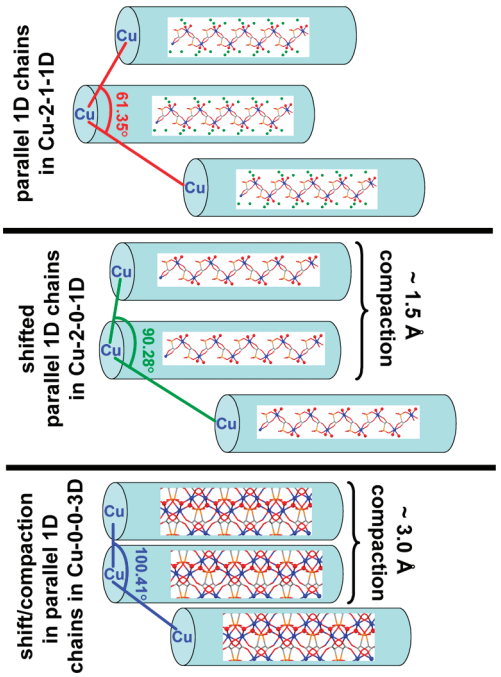

Figure 9. Chain "slipping" and compaction during the dehydration of **Cu-L-2-1-1D** to **Cu-L-2-0-1D** to **Cu-L-0-0-0D**.

Removal of Cu-bound waters from **Cu-L-2-0-1D** causes a further compaction of the interchain space in **Cu-L-0-0-3D**; see Figure 8, right. Intrachain Cu···Cu distances (5.730 Å) are virtually identical to the precursor 1D chain compounds. The same observation can be made as well for the interchain Cu···Cu distances (5.468 Å) parallel to the *b* axis. As expected the interchain Cu···Cu distances (3.741 Å) that are generated by chain compaction have been profoundly shortened. A dramatic, ~5.3 Å *c*-axis length reduction from 17.011(1) Å in **Cu-L-2-0-1D**, to 11.731(1) Å in **Cu-L-0-0-3D** is observed.

These profound changes in the way the chains interact also cause a substantial horizontal shift of a "layer" of 1D chains parallel to the *b* axis. Thus, the Cu−Cu−Cu angle changes from 61.35° in **Cu-L-2-1-1D**, to 90.28° in **Cu-L-2-0-1D**, to 100.41° in **Cu-L-0-0-3D**. This "slipping" process is schematically shown in Figure 9.

Transformation Pathway of Hydrated Cu-L-2-1-1D to Anhydrous Cu-L-0-0-3D. The conversion from **Cu-L-2-1-1D** → **Cu-L-0-0-3D** is irreversible. Exposure of **Cu-L-0-0-3D** to humid atmosphere or to liquid water does not cause the reverse conversion to **Cu-L-2-1-1D** or **Cu-L-2-1-1D**. This is not unexpected, as **Cu-L-0-0-3D** exhibits a very dense and compact structure. By carefully studying the crystal structure of **Cu-L-2-1-1D** and **Cu-L-0-0-3D** significant information can be extracted in order to rationalize the conversion **Cu-L-2-1-1D** → **Cu-L-0-0-3D**. Dehydration of **Cu-L-2-1-1D**, as demonstrated above, starts by removal of the water of crystallization to yield **Cu-L-2-0-1D**. However, this step is

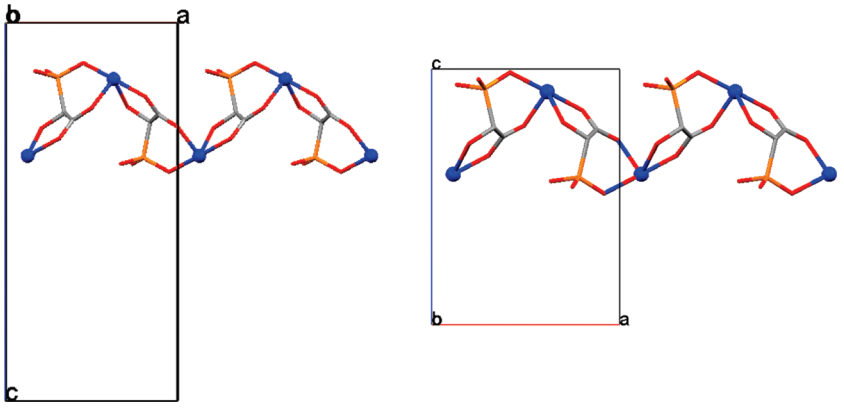

Figure 10. Generation of an "intermediate" 1D chain in the structure of **Cu-L-2-1-1D** after removal of Cu-bound waters (left image) and in the 3D structure of **Cu-L-0-0-3D** (right image).

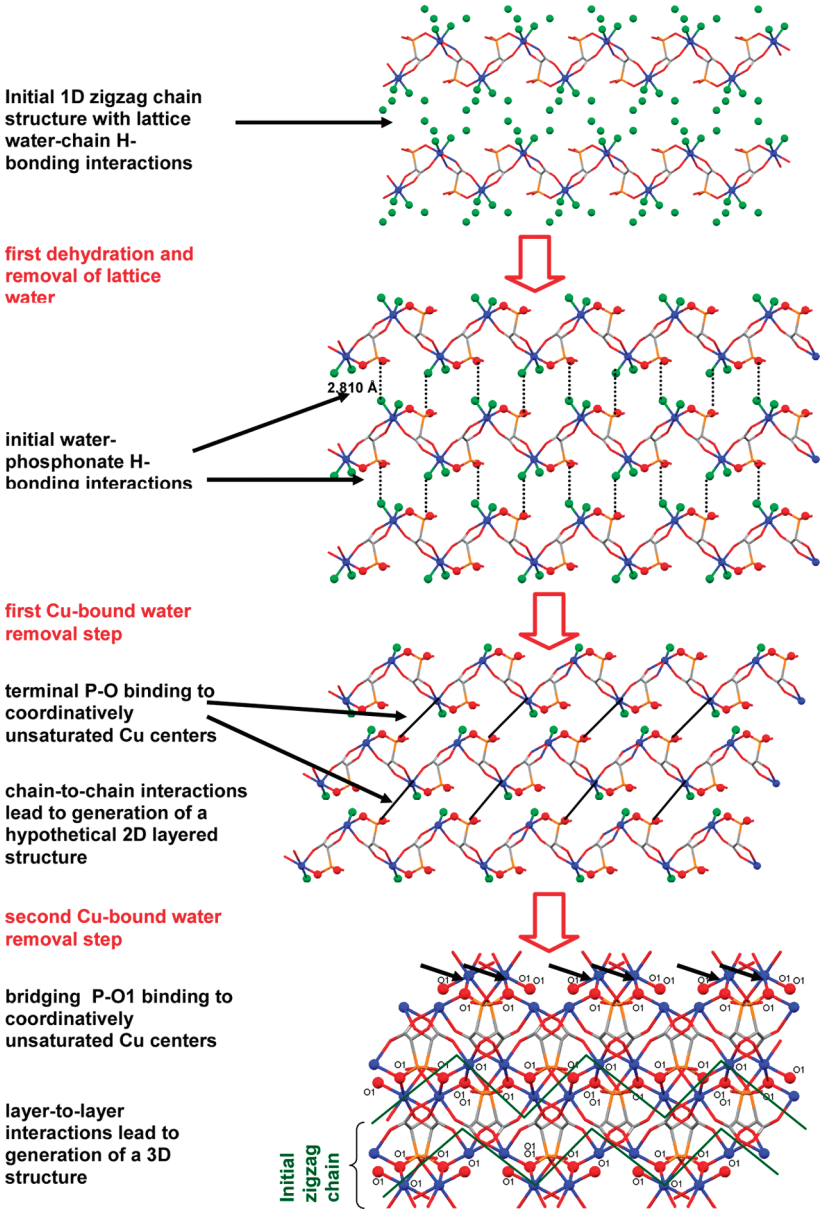

Figure 11. Proposed pathway for the **Cu-L-2-1-1D** → **Cu-L-2-0-1D** → **Cu-L-0-0-3D** conversion. The Cu-bound water molecules that are removed are highlighted in green.

indistinguishable (by TGA) from the second important step of removal of the two Cu-coordinated water molecules. In order to visualize that we have omitted the Cu-bound water molecules from the 1D structure of **Cu-L-2-1-1D**; see Figure 10 left. This generates an "intermediate" chain (along the *a* axis) with two coordinated sites on the Cu center in a *cis* arrangement. This "intermediate" chain also exists in the 3D structure of **Cu-L-0-0-3D**; see Figure 10 right. The two coordination sites generated on Cu after removal of the water molecules in **Cu-L-2-1-1D** (or in **Cu-L-2-0-1D**) are occupied by two phosphonate oxygens (O1 and O3) in the structure of **Cu-L-0-0-3D**. O(1) is already coordinated to Cu in the "intermediate" chain but now acts as a bridge between two Cu ions in the structure of **Cu-L-0-0-3D**. Concurrently, O(3) (which is not coordinated in the "intermediate" chain) is found coordinated to a neighboring Cu atom. These two Cu−O(phosphonate) interactions are responsible for the formation of a 3D structural motif.

In the structure of **Cu-L-2-1-1D** the noncoordinated phosphonate oxygen that binds to Cu in a terminal fashion after dehydration (O(3)) is found to form a strong hydrogen bond (2.810 Å) with a Cu-bound water molecule of a neighboring chain. This places the phosphonate oxygen in close proximity to the water molecule that upon its removal will leave a vacant site for it. We propose that this is the first step of formation of **Cu-L-0-0-3D**. This initial phosphonate binding to a neighboring chain then creates a 2D structure. Again, by closely looking at the structure of **Cu-L-2-1-1D**, one can see that the phosphonate oxygen that is already coordinated to Cu (and part of a 6-membered chelate ring) is located 4.013 Å away from the second Cu-bound water molecule to be removed. Analogously, the same Cu-bound phosphonate oxygen in the structure of **Cu-L-2-0-1D** is 3.803 Å away from the second Cu-bound water molecule to be removed. Although these distances are far from being hydrogen bonds, it is obvious that after initial Cu-phosphonate binding takes place during the first step mentioned above

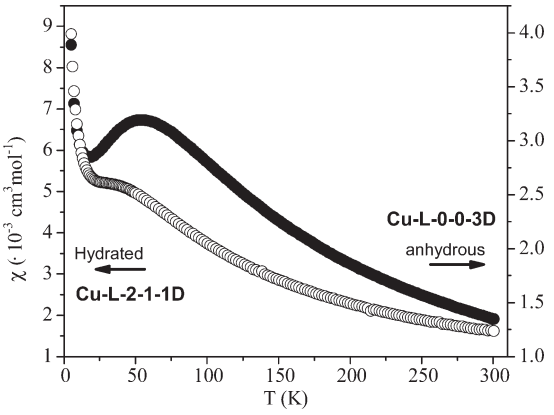

Figure 12. Temperature dependence of molecular magnetic susceptibility χ for the "hydrated" **Cu-L-2-1-1D** (open circles) and "anhydrous" **Cu-L-0-0-3D** (full circles) compounds.

(with concomitant formation of the 2D motif) this phosphonate oxygen will approach a Cu atom coming from a neighboring "layer", thus generating a 3D structure. We propose this to be the final step of the **Cu-L-2-1-1D** → **Cu-L-2-0-1D** → **Cu-L-0-0-3D** transformation. Collectively, these stepwise processes are shown in Figure 11.

Magnetic and EPR Studies. Magnetic susceptibility measurements and EPR spectra were carried out on powdered samples of the "hydrated" **Cu-L-2-1-1D** and "anhydrous" **Cu-L-0-0-3D** compounds. Magnetics data are shown in Figure 12. For the "hydrated" complex the room temperature value of χT is 0.486 cm^3 K mol^{-1}. The temperature dependence of χ exhibits a relatively broad maximum at ca. 35−40 K. Below 25 K an abrupt increase of χ is observed. The behavior of χ above 25 K is consistent with antiferromagnetic interactions. The structural motif of **Cu-L-2-1-1D** is a 1D chain. For such systems the Bonner−Fischer approximation may be used in order to model the χ vs T data.[20] The maximum observed in the χ vs T plot is related with the magnitude of the exchange interaction J through the relationship $kT_{max}/|J| \approx 1.282$ ($H = -2J \Sigma \boldsymbol{S}_i \mathbf{S}_{i+1}$). From this, a value of -25 cm^{-1} is estimated for the *intra*-chain exchange interactions. The increase of χ below 25 K is attributed to the presence of monomeric impurities.

For compound **Cu-L-0-0-3D** the room temperature χT = 0.400 cm^3 K mol^{-1}. The χ vs T diagram exhibits a maximum at around 60 K indicative of antiferromagnetic interactions. The abrupt increase below 15 K is attributed to paramagnetic impurities.

Collectively, the magnetics and EPR data are consistent with antiferromagnetic interactions, but these cannot be used to prove the 1D → 3D transformation, which was unequivocally proven by the structural study. A detailed account of the magnetics and EPR data is given in Supporting Information.

Conclusions

The topotactic transformation of 1D **Cu-L-2-1-1D** hybrid to 3D **Cu-L-0-0-3D** occurs via a stepwise pathway. The initial step is removal of lattice water to give 1D **Cu-L-2-0-1D**. Lattice water molecules in **Cu-L-2-1-1D** interact with neighboring chains through a complicated hydrogen bonding network. Therefore, once the lattice water is removed profound changes in hydrogen bonding interactions (chain···H_2O··· chain) ensue. Vacating the interchain space causes the chains to compact and "slip", with concomitant creation of a new hydrogen bonding scheme (chain···chain). The initial zigzag 1D chain is retained throughout the dehydration process. In 3D **Cu-L-0-0-3D** the vacant sites on Cu generated by removal of Cu-bound waters are now occupied by phosphonate oxygens from neighboring chains. We are currently extending this dehydration-induced chemistry to other metal-HPAA systems. Results will be reported in the near future.

Acknowledgment. The work at Heraklion was supported by a grant from the Research Committee of the University of Crete, ELKE, (KA 2573) and at Malaga by the MAT2006-11080-C2-1 research grant. We also thank Dr. M. Pissas for his assistance and useful discussions regarding the magnetic measurements.

Supporting Information Available: Crystallographic cif files for **Cu-L-2-1-1D**, **Cu-L-2-0-1D**, and **Cu-L-0-0-3D**, and a detailed account of all magnetics and EPR studies. This material is available free of charge via the Internet at http://pubs.acs.org.

References

(1) (a) Robson, R. *Dalton Trans.* **2008**, 5113–5131. (b) Rao, C. N. R.; Cheetham, A. K.; Thirumurugan, A. *J. Phys.: Condens. Matter* **2008**, *20*, item 083202. (c) Murugavel, R.; Choudhury, A.; Walawalkar, M. G.; Pothiraja, R.; Rao, C. N. R. *Chem. Rev.* **2008**, *108*, 3549–3655. (d) Ferey, G. *Dalton Trans.* **2009**, 4400–4415. (e) Kesanli, B.; Lin, W. *Coord. Chem. Rev.* **2003**, *246*, 305–326. (f) Kitagawa, S.; Kitaura, R.; Noro, S. *Angew. Chem., Int. Ed.* **2004**, *43*, 2334–2375. (g) Eddaoudi, M.; Moler, D. B.; Li, H. L.; Chen, B. L.; Reineke, T. M.; O'Keeffe, M.; Yaghi, O. M. *Acc. Chem. Res.* **2001**, *34*, 319–330. (h) Yaghi, O. M.; H. Li, L.; Davis, C.; Richardson, D.; Groy, T. L. *Acc. Chem. Res.* **1998**, *31*, 474–484. (i) Kaskel, S. In *Handbook of Porous Solids*; Schluth, F., Sing, K. S. W., Weitkamp, J., Eds.; Wiley-VCH: Weinheim, 2002; Vol. 2, pp 1190−1249. (j) Almeida Paz, F. A.; Klinowski, J. *Pure Appl. Chem.* **2007**, *79*, 1097–1110.

(2) (a) Chui, S.S.-Y.; Lo, S.M.-F.; Charmant, J. P. H.; Orpen, A. G.; Williams, I. D. *Science* **1999**, *283*, 1148–1150. (b) Lebedev, O. I.; Millange, F.; Serre, C.; Van Tendeloo, G.; Ferey, G. *Chem. Mater.* **2005**, *17*, 6525–6527. (c) Chen, B.; Eddaoudi, M.; Hyde, S. T.; O'Keeffe, M.; Yaghi, O. M. *Science* **2001**, *291*, 1021–1023. (d) Shimizu, G. K. H. *J. Solid State Chem.* **2005**, *178*, 2519–2526. (e) Tranchemontagne, D. J.; Ni, Z.; O'Keeffe, M.; Yaghi, O. M. *Angew. Chem., Int. Ed.* **2008**, *47*, 5136–5147.

(3) (a) Zhang, J.-P.; Chen, X.-M. *Chem. Commun.* **2006**, 1689–1699. (b) Banerjee, R.; Phan, A.; Wang, B.; Knobler, C.; Furukawa, H.; O'Keeffe, M.; Yaghi, O. M. *Science* **2008**, *319*, 939–943.

(4) (a) Hong, S.; Zou, Y.; Moon, D.; Lah, M. S. *Chem. Commun.* **2007**, 1707–1709. (b) Du, M.; Wang, X.-G.; Zhang, Z.-H.; Tang, L.-F.; Zhao, X.-J. *CrystEngComm* **2006**, *8*, 788–793. (c) Hong, M. *Cryst. Growth Des.* **2007**, *7*, 10–14. (d) James, S. L. *Chem. Soc. Rev.* **2003**, *32*, 276–288.

(5) (a) Mastalerz, M. *Angew. Chem., Int. Ed.* **2008**, *47*, 445–447. (b) Cote, A. P.; Benin, A. I.; Ockwig, N. W.; O'Keeffe, M.; Matzger, A. J.; Yaghi, O. M. *Science* **2005**, *310*, 1166–1170. (c) Tilford, R. W.; Gemmil, R.; zur Loye, H.-C.; Lavigne, J. J. *Chem. Mater.* **2006**, *18*, 5296–5301. (d) El-Kaderi, H. M.; Hunt, J. R.; Mendoza-Cortes, J. L.; Cote, A. P.; Taylor, R. E.; O'Keeffe, M.; Yaghi, O. M. *Science* **2007**, *316*, 268–272. (e) Niu, W.; Smith, M. D.; Lavigne, J. J. *J. Am. Chem. Soc.* **2006**, *128*, 16466–16467. (f) Niu, W.; O'Sullivan, C.; Rambo, B. M.; Smith, M. D.; Lavigne, J. J. *Chem. Commun.* **2005**, 4342–4344. (g) Hunt, J. R.; Doonan, C. J.; LeVangie, J. D.; Cote, A. P.; Yaghi, O. M. *J. Am. Chem. Soc.* **2008**, *130*, 11872–11873.

(6) (a) Schull, T. L.; Knight, D. A. *Coord. Chem. Rev.* **2005**, *249*, 1269–1282. (b) Matczak-Jon, E.; Videnova-Adrabinska, V. *Coord. Chem. Rev.* **2005**, *249*, 2458–2488. (c) Sergienko, V. S. *Russ. J. Coord. Chem.* **2001**, *27*, 681–710. (d) Clearfield, A. *Dalton Trans.* **2008**, 6089–6102. (e) Clearfield, A. In *Progress in Inorganic Chemistry*; Karlin, K. D., Ed.; John Wiley: New York, 1998; pp 371−510. (f) Meada, K. *Microporous Mesoporous Mater.* **2004**, *73*, 47–55. (g) Vioux, A.; Le Bideau, J.; Mutin, P. H.; Leclercq, D. *Top. Curr. Chem.* **2004**, *232*, 145–174.

(7) (a) Hix, G. B.; Turner, A.; Kariuki, B. M.; Tremayne, M.; MacLean, E. J. *J. Mater. Chem.* **2002**, *12*, 3220–3227. (b) Riou-Cavallec, M.; Sanselme, M.; Guillou, N.; Férey, G. *Inorg. Chem.* **2001**, *40*, 723–725. (c) Rabu, P.; Janvier, P.; Bujoli, B. *J. Mater. Chem.* **1999**, *9*, 1323–1326. (d) Distler, A.; Sevov, S. *Chem. Commun.* **1998**, 959–960. (e) Drumel, S.; Janvier, P.; Barboux, P.; Bujoli-Doeuff, M.; Bujoli, B. *Inorg. Chem.* **1995**, *34*, 148–156. (f) Demadis, K. D.; Anagnostou, Z.; Zhao, H. *ACS Appl. Mater. Interfaces* **2009**, *1*, 35–38. (g) Stock, N.; Stucky, G. D.; Cheetham, A. K. *Chem. Commun.* **2000**, 2277–2278. (h) Cabeza, A.; Aranda, M. A. G.; Bruque, S. *J. Mater. Chem.* **1998**, *8*, 2479–2485. (i) Stock, N.; Frey, S. A.; Stucky, G. D.; Cheetham, A. K. *J. Chem. Soc., Dalton Trans.* **2000**, 4292–4296. (j) Demadis, K. D.; Lykoudis, P.; Raptis, R. G.; Mezei, G. *Cryst. Growth Des.* **2006**, *6*, 1064–1067. (k) Hix, G. B.; Wragg, D. S.; Wright, P. A.; Morris, R. E. *J. Chem. Soc., Dalton Trans.* **1999**, 3359–3362. (l) Sanselme, M.; Riou-Cavallec, M.; Greneche, J. M.; Férey, G. *J. Solid State Chem.* **2002**, *164*, 354–360. (m) Demadis, K. D.; Papadaki, M.; Raptis, R. G.; Zhao, H. *J. Solid State Chem.* **2008**, *181*, 679–683. (n) Demadis, K. D.; Papadaki, M.; Raptis, R. G.; Zhao, H. *Chem. Mater.* **2008**, *20*, 4835–4846. (o) Gomez-Alcantara, M. M.; Aranda, M. A. G.; Olivera-Pastor, P.; Beran, P.; Garcia-Munoz, J. L.; Cabeza, A. *Dalton Trans.* **2006**, 577–585. (p) Cunha-Silva, L.; Ananias, D.; Carlos, L. D.; Almeida Paz, F. A.; Rocha, J. *Z. Kristallogr.* **2009**, *224*, 261–272.

(8) (a) Zhiming Duan, Z.; Zhang, Y.; Zhang, B.; Zhu, D. *J. Am. Chem. Soc.* **2009**, *131*, 6934–6935. (b) Campo, J.; Falvello, L. R.; Mayoral, I.; Palacio, F.; Soler, T.; Tomás, M. *J. Am. Chem. Soc.* **2008**, *130*, 2932–2933. (c) Ene, C. D.; Madalan, A. M.; Maxim, C.; Jurca, B.; Avarvari, N.; Andruh, M. *J. Am. Chem. Soc.* **2009**, *131*, 4586–4587. (d) Zhang, Y.-J.; Liu, T.; Kanegawa, S.; Sato, O. *J. Am. Chem. Soc.* **2009**, *131*, 7942–7943. (e) Wang, Z. M.; Zhang, B.; Fujiwara, H.; Kobayashi, H.; Kurmoo, M. *Chem. Commun.* **2004**, 416–417. (f) Kurmoo, M.; Kumagai, H.; Chapman, K. W.; Kepert, C. J. *Chem. Commun.* **2005**, 3012–3014. (g) Armentano, D.; DeMunno, G.; Mastropietro, T. F.; Julve, M.; Lloret, F. *J. Am. Chem. Soc.* **2005**, *127*, 10778–10779. (h) Halder, G. J.; Kepert, C. J. *Aust. J. Chem.* **2006**, *59*, 597–604. (i) Vittal, J. J. *Coord. Chem. Rev.* **2007**, *251*, 1781–1795. (j) Cheng, X. N.; Zhang, W. X.; Chen, X. M. *J. Am. Chem. Soc.* **2007**, *129*, 15738–15739. (k) Cheng, X. N.; Zhang, W. X.; Lin, Y. Y.; Zheng, Y. Z.; Chen, X. M. *Adv. Mater.* **2007**, *19*, 1494–1498. (l) Neville, S. M.; Halder, G. J.; Chapman, K. W.; Duriska, M. B.; Southon, P. D.; Cashion, J. D.; Letard, J.-F.; Moubaraki, B.; Murray, K. S.; Kepert, C. J. *J. Am. Chem. Soc.* **2008**, *130*, 2869–2876.

(9) (a) Svoboda, J.; Zima, V.; Beneš, L.; Melánová, K.; Trchová, M.; Vlcek, M. *Solid State Sci.* **2008**, *10*, 1533–1542. (b) Zima, V.; Svoboda, J.; Beneš, L.; Melánová, K.; Trchová, M.; Dybal, J. *J. Solid State Chem.* **2007**, *180*, 929–939.

(10) Colodrero, R. M. P.; Cabeza, A.; Olivera-Pastor, P.; Infantes-Molina, A.; Barouda, E.; Demadis, K. D.; Aranda, M. A. G. *Chem.—Eur. J.* **2009**, *15*, 6612–6618.

(11) Lodhia, S.; Turner, A.; Papadaki, M.; Demadis, K. D.; Hix, G. B. *Cryst. Growth Des.* **2009**, *9*, 1811–1822.

(12) Boultif, A.; Louer, D. *J. Appl. Crystallogr.* **2004**, *37*, 724–731.

(13) Wolff, P. M. *J. Appl. Crystallogr.* **1968**, *1*, 108–113.

(14) Smith, G. S.; Snyder, R. L. *J. Appl. Crystallogr.* **1979**, *12*, 60–65.

(15) Altomare, A.; Burla, M. C.; Camalli, M.; Carrozzini, B.; Cascarano, G. L.; Giacovazzo, C.; Guagliardi, A.; Moliterni, A. G. G.; Polidori, G.; Rizzi, R. *J. Appl. Crystallogr.* **1999**, *32*, 339–340.

(16) Rietveld, H. M. *J. Appl. Crystallogr.* **1969**, *2*, 65–71.

(17) (a) Toby, B. H. *J. Appl. Crystallogr.* **2001**, *34*, 210–213. (b) Larson, A. C.; von Dreele, R. B. *Los Alamos National Lab. Report No. LA-UR-86−748*, **2000**.

(18) Dollase, W. A. *J. Appl. Crystallogr.* **1986**, *19*, 267–272.

(19) (a) Danilich, M. J.; Burton, D. J.; Marchant, R. E. *Vibr. Spectrosc.* **1995**, *9*, 229–234. (b) Chaplais, G.; Le Bideau, J.; Leclercq, D.; Vioux, A. *Chem. Mater.* **2003**, *15*, 1950–1956. (c) Demadis, K. D.; Katarachia, S. D. *Phosphorus Sulfur Silicon* **2004**, *179*, 627–640. (d) Kim, C. S.; Lad, R. J.; Tripp, C. P. *Sensors Actuators B* **2001**, *76*, 442–448.

(20) Kahn, O. *Molecular Magnetism*; VCH Publishers: Weinheim, 1993.